materials

MDPI

Article

The Nature-Inspired Metaheuristic Method for Predicting the Creep Strain of Green Concrete Containing Ground Granulated Blast Furnace Slag

Łukasz Sadowski [1,*], Mehdi Nikoo [2], Mohd Shariq [3], Ebrahim Joker [4] and Sławomir Czarnecki [1]

1 Faculty of Civil Engineering, Wroclaw University of Science and Technology, WybrzezeWyspiańskiego 27, 50-370 Wroclaw, Poland; slawomir.czarnecki@pwr.edu.pl
2 Young Researchers and Elite Club, Ahvaz Branch, Islamic Azad University, Ahvaz, Iran; sazeh84@yahoo.com
3 Department of Civil Engineering, Aligarh Muslim University, Aligarh 202001, India; mshariqdce@gmail.com
4 Department of Civil Engineering, Dariun Branch, Islamic Azad University, Dariun, Iran; joker_ebrahim@yahoo.com
* Correspondence: lukasz.sadowski@pwr.edu.pl

Received: 12 November 2018; Accepted: 15 January 2019; Published: 17 January 2019

Abstract: The aim of this study was to develop a nature-inspired metaheuristic method to predict the creep strain of green concrete containing ground granulated blast furnace slag (GGBFS) using an artificial neural network (ANN)model. The firefly algorithm (FA) was used to optimize the weights in the ANN. For this purpose, the cement content, GGBFS content, water-to-binder ratio, fine aggregate content, coarse aggregate content, slump, the compaction factor of concrete and the age after loading were used as the input parameters, and in turn, the creep strain (ε_{cr}) of the GGBFS concrete was considered as the output parameters. To evaluate the accuracy of the FA-ANN model, it was compared with the well-known genetic algorithm (GA), imperialist competitive algorithm (ICA) and particle swarm optimization (PSO). Results indicated that the ANNs model, in which the weights were optimized by the FA, were more capable, flexible and precise than other optimization algorithms in predicting the ε_{cr} of GGBFS concrete.

Keywords: concrete; ground granulated blast furnace slag; creep strain; artificial neural networks; firefly algorithm

1. Introduction

The time-dependent deformation of concrete, as a result of creep strains, severely affects the durability of concrete structures. As stated by El-Shafie and Aminah [1], the stochastic nature of creep deformation and its reliance on a large number of uncontrolled parameters (e.g., relative humidity, time of load application, stress level) makes the process of the prediction and development of accurate mathematical models very difficult (almost impossible). Thus, due to the great number of variable and uncertain parameters. As pointed out by Hołowaty [2], current empirically based models in design codes are too simplified, and therefore the real-time behavior of concrete structures is still not fully understood.

The creep strain (ε_{cr}) depends primarily on the composition of the concrete. This composition has recently been more frequently modified using eco-friendly admixtures. The concrete obtained applying these kinds of admixtures are usually known as "green concrete". One example of these admixtures is ground granulated blast furnace slag (GGBFS). GGBFS is a fine powder obtained by grinding the blast furnace by-product of the steel industry [3]. The application of GGBFS in sustainable cement

based materials is usually beneficial. This is mainly due to a slower hydration rate in comparison with ordinary Portland cement, and also the decrease in the emission of CO_2. However, there is lack of research on the influence of GGBFS at creep in literature. In some cases, the application of GGBFS in cement-based materials lowers the creep strain, whereas in others the creep strain is higher in comparison with concrete made of ordinary Portland cement [3,4]. Many prediction models have been proposed for assessing the creep of ordinary concrete [5–10]. Due to the intensive development of the application of GGBFS, these prediction models are not adequate for GGBFS based concrete. The actual prediction models are not able to reproduce the behavior of concrete, for which a high part of the cement is replaced by slag. However, new models have been developed in order to consider the influence of slag on the properties of concrete [11].

The conventional approach to calculate the ε_{cr} requires a series of laboratory tests to be performed. These tests are expensive and time-consuming. Thus, each possibility of a less expensive and faster prediction of the ε_{cr} of GGBFS concrete may be very useful for designing reinforced and pre-stressed concrete structures. This might be done based on the information concerning the composition of the concrete mixture and/or the values of the selected rheological properties. Artificial neural networks (ANNs) can be especially useful for this purpose. ANNs are artificial models of the biological connection and cooperation between the brain and the rest of the body. They very often work in a similar manner to human cells, using a one-way signal flow. The main advantage of ANNs is that they can handle a large amount of datasets. The use of ANNs is also beneficial due to their ability to detect complex relationships between independent variables. The method based on ANNs can be utilized as a supplementary tool for creep strain prediction. Thanks to the application of ANNs, the series of expensive and time-consuming tests may not be necessary.

Several researchers have recently tried to predict the ε_{cr} in concrete using ANN models. For example, Karthikeyan et al. [12] and Gedam et al. [13] predicted the creep of high performance concrete (HPC). Baland and Bodin [14] used the nonparametric ANN model for this purpose. However, most of the attempts were performed based on the simplest back propagation ANN model (e.g., the Widrow–Hoff algorithm in [15], Levenberg–Marquardt algorithm in [12]). Recently, the intensive development of the application of more advanced optimization algorithms in ANNs has been noted in the prediction of properties of green (eco) concrete [16,17]. It includes the use of genetic algorithms (GA), which have recently been used for predicting the compressive strength of concrete [18], the displacement of floors [19], the elastic modulus of recycled aggregate concrete [20,21] or the coefficient of safety in soil stabilization [22]. Multi-objective genetic programming has been used successfully by Gandomi et al. [23] in concrete creep formulation. The imperialist competitive algorithm (ICA), particle swarm optimization (PSO) and firefly algorithm (FA) are also getting more attention [24]. These algorithms are usually used to improve the learning processes of ANNs. Thus, in this article, the authors decided to use the FA for this purpose.

The firefly is a very interesting insect, and their spectacular plays have inspired poets and scientists. Many researchers have studied the behavior of fireflies in nature [24]. The nature-inspired FA is a metaheuristic algorithm proposed by Xin-She Yang [25] and inspired by the flashing behavior of fireflies. In the standard firefly algorithm, two important issues need to be defined. According to [24], the intensity of light is defined as:

$$I(r) = I_0 e^{-\gamma r^2}, \quad (1)$$

where I_0 represents the intensity of the source light and the absorption of light by approximating the constant coefficient of light absorption γ.

The intensity of light I is referred to as an absolute measure of emitted light by the firefly, while the attractiveness β is the measure of light seen by the other fireflies and defined by Equation (2):

$$\beta = \beta_0 e^{-\gamma r^2}, \quad (2)$$

Where β_0= the attractiveness at the Euclidean distance r is defined by Equation (3) between two fireflies s_i and s_j, and is equal to 0:

$$r_{ij} = ||s_i - s_j|| \sqrt{\sum_{k=1}^{k=n} \left(s_{ik} - s_{jk}\right)^2} \quad (3)$$

According to Equations (1) and (2), there are two asymptotic behaviors of the FA. If $\gamma \to 0$, the attractiveness is constant ($\beta = \beta_0$), and if $\gamma \to \infty$, the firefly movement becomes a random walk.

The FA is being more frequently used in civil engineering applications. For example, Bui et al. [26] used the FA in a modified ANN model based expert system for predicting the compressive and tensile strength of high-performance concrete. Moreover, Sheikholeslami et al. [27] used an improved FA with an upper bound strategy to optimize reinforced concrete retaining walls. Additionally, Nigdeli et al. [28] found this method useful to optimize reinforced concrete footings.

To the best of our knowledge, there is no developed method for predicting the creep strain of concrete with ground granulated blast furnace slag using the FA. Thus, this study aims to apply the FA in order to optimize the weights of an ANN model for determining the creep strain of GGBFS concrete. The obtained results were validated using the well-known GA, ICA and PSO.

2. Experimental Setup

2.1. Materials

Locally available ordinary 43 grade (C43) Portland cement (OPC) and the commercially available GGBFS were used in the experiments (Indorama cement industry, Raipur, Maharashtra, India). The physical properties are presented in Table 1, while the selected chemical properties of the cement and GGBS are given in Table 2 (IS 8112, 1989 [29] and IS 12089, 1999 [30]), respectively.

Table 1. Physical properties of the cement and ground granulated blast furnace slag (GGBFS).

Characteristic	Experimental Value	
	Cement	GGBFS
Blaine's fineness (m^2/kg)	245	340
Specific gravity	3.15	2.86
Soundness (mm)	1.5	1.5
Compressive strength (MPa)	45.9	40 (with 30% GGBFS)
Normal Consistency (%)		
OPC + 0% GGBFS	27.0	
OPC + 20% GGBFS	28.5	
OPC + 40% GGBFS	29.5	
OPC + 60% GGBFS	31.00	

Table 2. Chemical properties of the cement and ground granulated blast furnace slag (GGBFS).

Name of Oxide	Cement (%)	GGBFS
CaO	63.71	38.01
SiO_2	22.18	37.88
Al_2O_3	07.35	14.23
Fe_2O_3	03.82	0.38
MgO	0.95	9.1
Na_2O	0.28	0.26
K_2O	0.11	0.15
P_2O_5	0.05	0.01
TiO_2	0.27	0.34
MnO	0.04	0.07
Glass content	-	91.0

The particle size distribution of the OPC and GGBFS was carried out using the Malvern particle size analyzer, which has Helium-Neon laser rays with a micron range of 0.5 to 560. Isopropyl alcohol

with sodium pyrophosphate was used for the dispersion of particles. The cement and GGBFS were stored in airtight silos to protect them from moisture. The test results of the particle size distribution of the OPC and GGBFS are given in Figure 1.

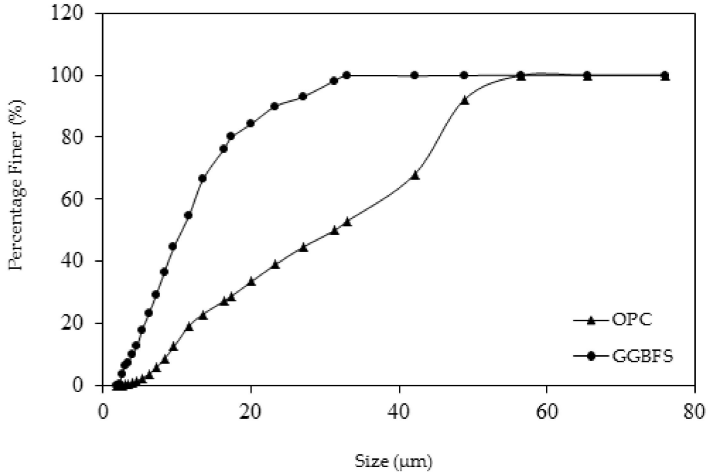

Figure 1. Particle size distribution of the ordinary Portland cement and ground granulated blast furnace slag.

Locally available natural river sand with a fineness modulus of 2.45 was used as the fine aggregate. The particle size distribution of the sand is given in Figure 2a. Locally available crushed stone basalt aggregate with a maximum nominal size of 16 mm and a fineness modulus of 6.8 was used as the coarse aggregate. The sieve analysis is given in Figure 2b.

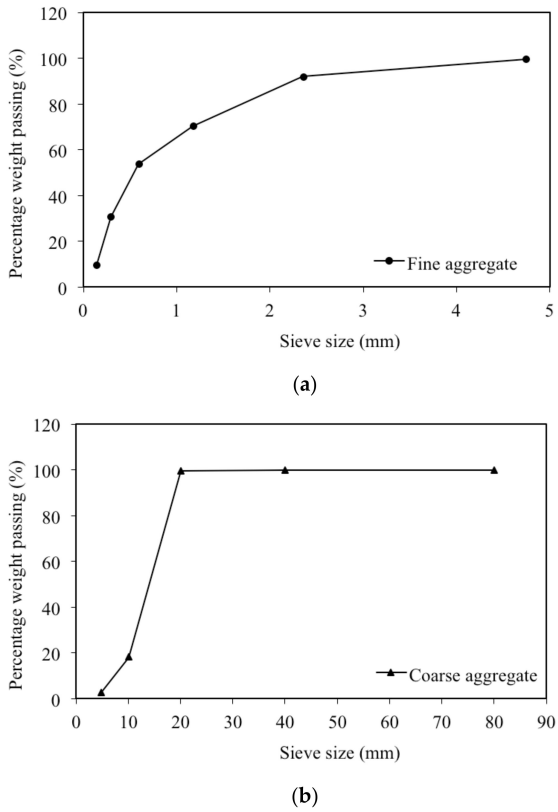

Figure 2. Particle size distribution of: (**a**) Fine aggregate; (**b**) Coarse aggregate.

Initially, based on the method of trial, three OPC concrete mixes were prepared with a target compressive strength of 45 MPa, 35 MPa and 25 MPa. Five specimens from each mix were tested at the age of 7 and 28 days for the OPC concrete mix proportioning. GGBFS concrete mixes were also prepared and had a cement replacement ratio of 20%, 40% and 60%. The water-to-binder ratio changed from 0.45 to 0.55. Thus, there were three mix groups designated as M1, M2 and M3 containing four concrete mixes in each mix group i.e., a total of twelve concrete mixes were prepared. In all the concrete mixes, the fine to coarse aggregate ratio was kept constant at 0.6 while verifying the maximum density of the combined aggregate. Table 3 shows the details of the concrete mix proportions.

Table 3. Concrete mix proportions.

Mix Group	Mix Designation	Cement (kg/m^3)	GGBFS (kg/m^3)	Aggregates (kg/m^3)		Water-Binder Ratio
				Fine	Coarse	
M1	M10	400	0	665	1107	0.45
	M11	320	80			
	M12	240	160			
	M13	160	240			
M2	M20	350	0	680	1132	0.50
	M21	280	70			
	M22	210	140			
	M23	140	210			
M3	M30	320	0	688	1145	0.55
	M31	256	64			
	M32	192	128			
	M33	128	192			

2.2. Methods

The experiments were performed in a laboratory in order to determine the creep strain of the plain and GGBFS concrete. Creep strain can be defined as the gradual increase in strain induced by the constant sustained loading applied on the concrete specimen, and can be denoted as ε_{cr}. The sustained loading was applied for 150 days on 150 × 600 mm cylindrical specimens to investigate the ε_{cr} of the GGBFS concrete. As pointed out previously by Shariq et al. [31], ε_{cr} can be defined as:

$$\varepsilon_{cr} = \frac{(\delta l_t)_c}{l} \quad (4)$$

where ε_{cr} = creep strain[μm/m]; $(\delta l_t)_c$ = length changes in time due to creep [μm]; l = original length[m].

Two specimens of each mix were prepared for the creep tests. The prepared concrete specimens for the measurement of creep strain are shown in Figure 3a. For the measurement of creep, the specimen was loaded at the age of 28 days for each mix at a sustained load level of 50% of the first crack load (i.e., 20, 17 and 12 ton for M10, M20 and M30 plain concrete mixes, respectively). Before loading the creep specimens, the first crack load of the plain concrete specimen after 28 days of curing was measured on a compression testing machine, and the same load was applied for the GGBFS based concrete specimen for each mix. Hence, the stress level on the GGBFS concrete specimens was also 50% of the first crack load measured on the plain concrete specimens (i.e., 20, 17 and 12 ton for respective GGBGFS concrete mixes). A hydraulic jack was used to apply the sustained load, which was maintained through the proving ring. For each mix, the total deformation was observed at 1, 3, 7, 14, 21, 28, 30, 56, 60, 90, 120 and 150 days. The creep specimens under a sustained loading condition are shown in Figure 3b. The creep strain for a given mix was obtained as the average of the strains recorded for two specimens. All the tests were performed at an ambient temperature of 27 ± 2 °C and relative humidity of 60–65%, as recommended for laboratory conditions for Indian standards (IS 516, 1999 [32]).

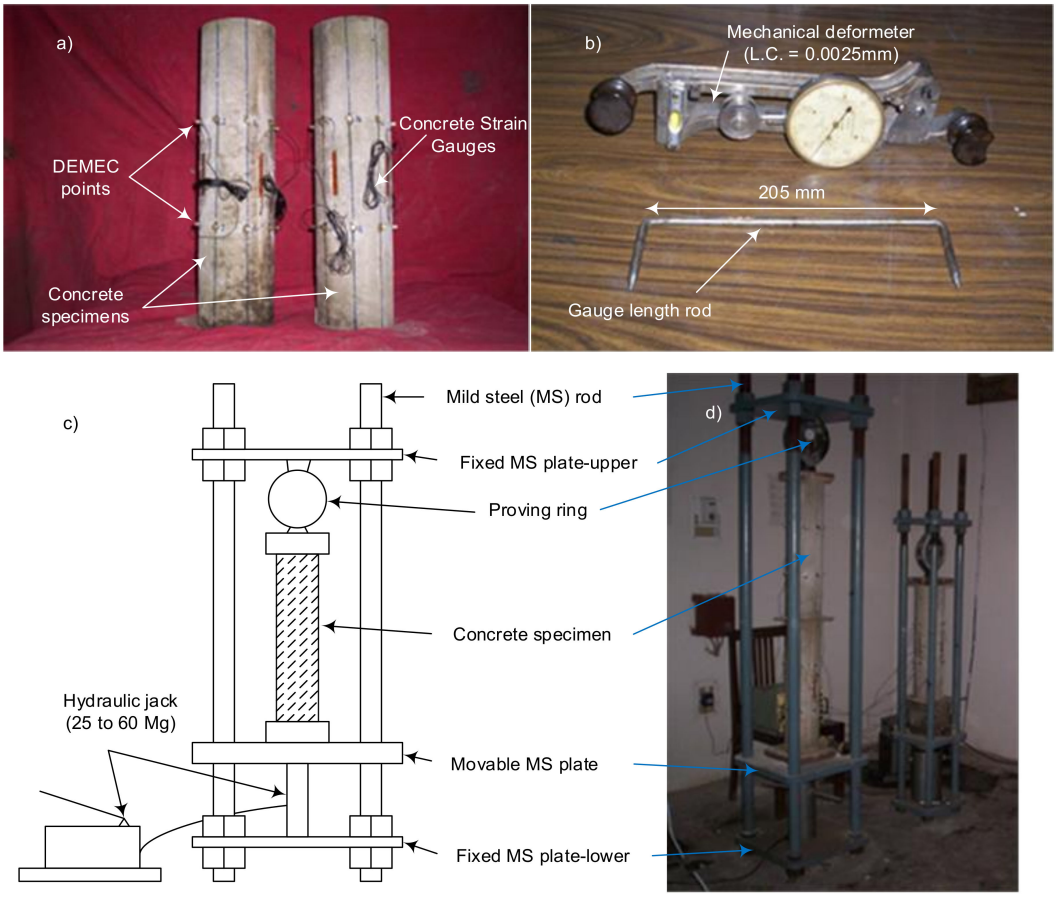

Figure 3. View of: (**a**) Prepared concrete specimens for creep strain measurement;(**b**) mechanical deformeter; (**c**) scheme of creep strain test setup; (**d**) creep strain specimens during the tests.

On the surface of each of the creep specimen, 6 gauge lines of demountable mechanical gauge (DEMEC) points were attached at a gauge length of 205 mm in a longitudinal direction. The DEMEC gauge had countersunk holes to facilitate the mounting of a Huggenberger deformeter (Figure 3c). The size of the countersink was of at least 0.0025 mm. Four concrete strain gauges were also pasted on each of the specimens to determine the creep strain by means of a digital strain indicator (Figure 3d) in order to cross check the results. Concrete strains were measured using a 65 mm gauge length with four sets of gauge points oriented at 90° along the sides of the cylinder.

Shrinkage strain was also measured on the concrete specimen of the same size as that considered in the creep strain measurement. The shrinkage strain was recorded at the same age as the creep strain was recorded i.e., at 1, 3, 7, 14, 21, 28, 56, 90, 120, 150 and 180 days. The shrinkage strain of each mix was recorded based on the average of two specimens from each mix. Then, the creep strain was calculated as creep strain = total strain – elastic strain due to instantaneous load—shrinkage strain. The results were presented by Shariq et al. [31].

2.3. Statistical Analysis of the Database

The data was collected from a previous study carried out by [31,33]. Table 4 shows several tens out of 132 values of parameters obtained experimentally. Table 5 shows the statistical characteristics of the measured parameters.

Table 4. Exemplary database (based on [31,33]).

No.	Age *t* (days)	Cement Content *C*(kg/m^3)	GGBFS Content *G*(kg/m^3)	Water-to-Binder Ratio w/b (-)	Fine Aggregate Content *Fa* (kg/m^3)	Coarse Aggregate Content *Ca* (kg/m^3)	Slump *S*(mm)	Compaction Factor *CF* (-)	Creep Strain ε_{cr}(*μm/m*)
1	0	400	0	0.45	665	1107	41	0.9	106
2	1	400	0	0.45	665	1107	41	0.9	123
3	3	400	0	0.45	665	1107	41	0.9	145
4	7	400	0	0.45	665	1107	41	0.9	162
5	14	400	0	0.45	665	1107	41	0.9	181
6	21	400	0	0.45	665	1107	41	0.9	196
7	28	400	0	0.45	665	1107	41	0.9	204
8	56	400	0	0.45	665	1107	41	0.9	235
9	90	400	0	0.45	665	1107	41	0.9	261
⋮	⋮	⋮	⋮	⋮	⋮	⋮	⋮	⋮	⋮
132	150	128	192	0.55	688	1145	61	0.96	937

Table 5. Statistical characteristics of the database.

Symbol and Name of Parameter	Statistical Characteristics			Standard Deviation	Shapiro–Wilk Test Results *W*
	Mean	Minimum	Maximum		
t - age after loading (days)	44.54	0.00	150.00	50.26	0.796
C - cement content (kg/m^3)	249.67	128.00	400.00	83.67	0.905
G – GGBFS content (kg/m^3)	107.00	0.00	240.00	80.70	0.793
w/b – water-to-binder ratio (-)	0.50	0.45	0.55	0.04	0.769
Fa - fine aggregate content (kg/m^3)	677.67	665.00	688.00	9.53	0.767
Ca - coarse aggregate content (kg/m^3)	1128.00	1107.00	1145.00	15.77	0.937
S - slump (mm)	50.33	41.00	61.00	5.78	0.834
CF - compaction factor (-)	0.92	0.90	0.96	0.02	0.935
ε_{cr}-creep strain (μm/m)	358.98	106.00	937.00	172,55	0.937

In order to determine the input variables for the ANN model, or their influence on the output value, the correlation between the input variables and output variable needed to be calculated. Before that, it was necessary to choose the proper test of correlation and to know the distribution of the input variables. For this purpose, it was useful to use the Shapiro–Wilk test of compliance with normal distribution. Using this test, the values of variables are ranked in a non-significant sequence, and then the test statistic is performed. According to [34], if the probability level in this statistic is lower than the determined significance level $W(\alpha)$, the hypothesis of conformity with normal distribution should be rejected. For all the measured parameters, the Shapiro–Wilk compliance test with normal distribution was conducted according to[34]:

$$W = \frac{\left(\sum_{i=1}^{n} a_i x_{(i)}\right)^2}{\sum_{i=1}^{n}(x_i - \overline{x})^2}, \quad (5)$$

where x_i is the sample number, $x_{(i)}$ is the i_{th}-smallest number in the sample and $\overline{x}$ is the sample mean. The results of the Shapiro–Wilk test for the individual parameters are shown in Table 5. In the Shapiro–Wilk test, if the level of *W* probability of this statistic drops below the determined level of the significance *W* = 0.956 of the test, the hypothesis of compliance with normal distribution is rejected. It can be concluded from Table 5 that for the predetermined level of significance α=0.01, the hypothesis regarding compliance of the distribution of all the parameters with normal distribution needed to be rejected for all of the parameters.

Thus, in order to analyze the correlation between the individual parameters and parameter ε_{cr}, the nonparametric Spearmann's (ρ_s) and Kendall's (τ) rank correlation coefficients were used. Moreover, the Fisher–Snedecor test was also conducted in order to confirm the above assumptions [35]. In this test, the *F* value at the level of significance α=0.05 should be higher than 3.91. The values of F < 3.91 means that the input variable has no effect on the creep strain value ε_{cr}. The calculation results of the ρ_s and τ rank correlation coefficients and the values of *F* are presented in Table 6.

Table 6. Results of Spearmann's (ρ_s) and Kendall's (τ) rank correlation coefficients and values of *F*.

Symbol and Name of Parameter	ρ_s	τ	*F*
t - age after loading (days)	0.597	0.453	66.34
C - cement content (kg/m^3)	0.788	0.612	13.14
G – GGBFS content (kg/m^3)	−0.473	−0.345	11.36
w/b – water-to-binder ratio (-)	0.282	0.199	27.17
Fa - fine aggregate content (kg/m^3)	0.437	0.342	27.16
Ca - coarse aggregate content (kg/m^3)	0.437	0.342	27.16
S - slump (mm)	0.437	0.342	27.25
CF - compaction factor (-)	0.543	0.405	26.67

Table 6 shows that correlation coefficients ρ_s and τ obtained the highest value for the parameters *t*, *C* and *CF*, which may indicate the major importance of these parameters in the selection of input variables for the ANN model. The negative values of correlation coefficients in the case of parameter *G* indicated a decrease in their values with an increase of the output variable ε_{cr}. On the other hand, the results of the Fisher–Snedecor test suggested that the most significant predictor could be *t* (with the *F* value over 66). Even the lowest values of coefficients ρ_s and τ were obtained for *w/b*, and the *F* value for this parameter was over 27 (much more than 3.91). According to [36], it has been proven that age after loading, as well as the parameters describing the components of the concrete responsible for the value of elastic modulus *E*, have the biggest impact on creep strain ε_{cr}. The results of the calculations of ρ_s and τ rank correlation coefficients and the Fisher–Snedecor test indicated the suitability of all the obtained parameters as input parameters for the ANN model. Considering the above, the input parameters for the ANN model were age after loading (*t*), cement content (*C*), GGBFS content (*G*), water-to-binder ratio (*w/b*), fine aggregate content (*Fa*), coarse aggregate content (*Ca*), slump (*S*) and compaction factor (*CF*).The creep strain ε_{cr} (μmm/mm) of the GGBFS concrete was used as the output parameter of this ANN model.

3. Numerical Analysis

3.1. Selection of the Optimum Structure of the ANN Model

Among the 132 data sets, 70% of the samples (92 sets) were used for training, 15% of the samples (20 sets) were selected for cross validation and the other 15% (20 sets) were used for network testing. According to [28], as well as to the guidelines advocated by Hecht-Nielson [37] and Rogers and Dowla [38], the number of nodes in the hidden layer should not be less than the value obtained from Equation (6)that was used for the maximum determination of the number of hidden layer nodes N_H:

$$N_H \leq min\left(2N_I + 1; \frac{N^{TR}}{N_I + 1}\right) \quad (6)$$

Where N_I is the number of input, and N^{TR} is the number of training samples. Given that the number of effective inputs is equal to 8, the maximum number of nodes in the hidden layer is 17 ($N_H \leq 17$), or given that the number of training samples is 92, the maximum number of nodes in the hidden layer is 10. The mean absolute error (MAE) was used for calculation and to select the most efficient topology of the ANN. The results are presented in Figure 4.

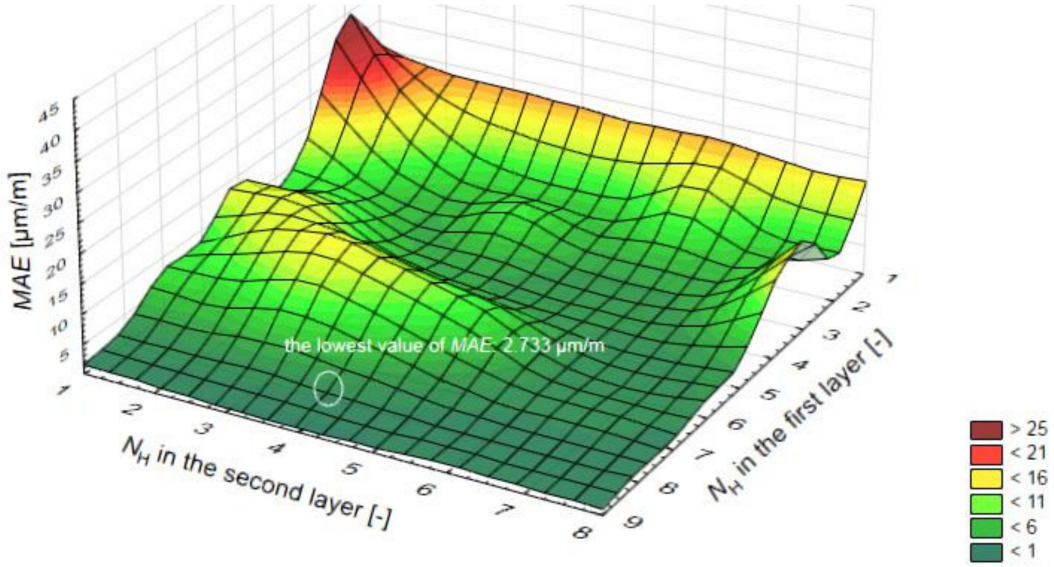

Figure 4. Results of mean absolute error (MAE) for different topologies of ANN models.

Finally, the topology of 8 input variables, 8 and 4 hidden layer nodes and 1 output variable with a MAE value of 0.80 was found to be the most accurate ANN model from all of the 72 ANN tested models. To determine the optimization of weights of each ANN model, the FA was used. In order for the models to properly function, and to determine the best one, the mean and the best criteria obtained from the models were compared with each other. According to the results, the feed forward (FF) model, in which the weights were optimized with the FA, offered the best results in the desired models through the 8-8-4-1 structure. The Tansig stimulation function and the Translim test algorithm were used in the final model. The optimum structure of the ANN model is shown in Figure 5.

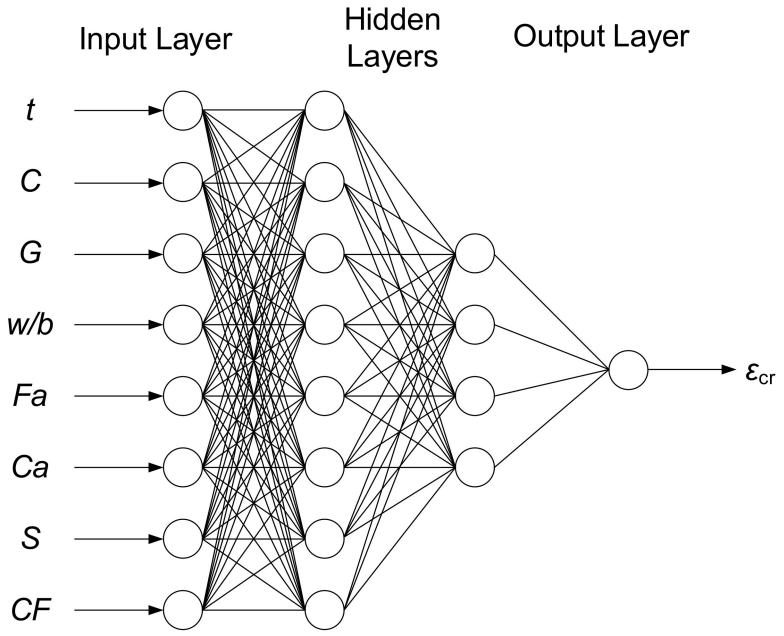

Figure 5. Optimum structure of the Artificial Neural Network model.

Figure 6 shows the cost graph for 50 iterations for the FA-ANN with the optimum 8-8-4-1 structure. This graph presents the minimum and best cost in two steps. If both parameters are closer to zero by

increasing the repetition, the accuracy of the model is higher. Moreover, if both parameters increase with repetition, the error rate in the model decreases.

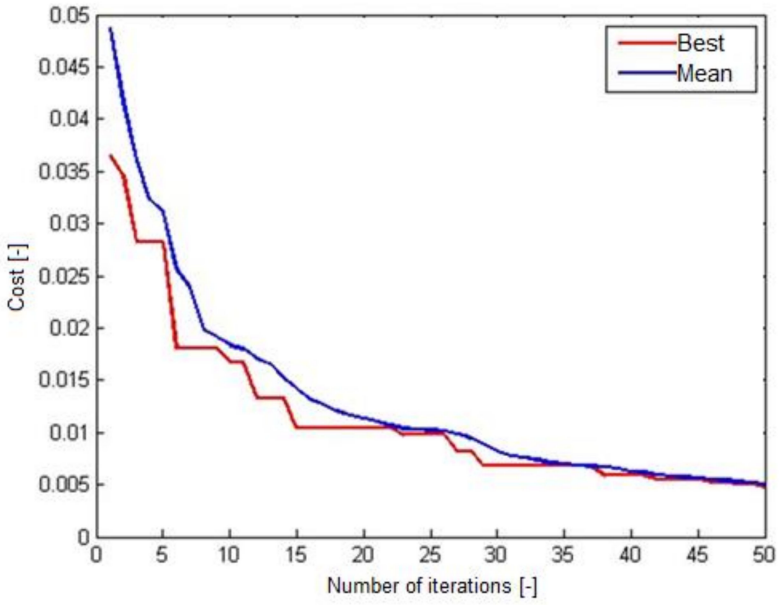

Figure 6. Chart in the FA-ANN with the optimum 8-8-4-1 structure.

Figure 7 shows the MSE performance in the FA-ANN with the optimum 8-8-4-1 structure for the training, cross-validation and test steps. According to this figure, the best performance was achieved at epoch 7.

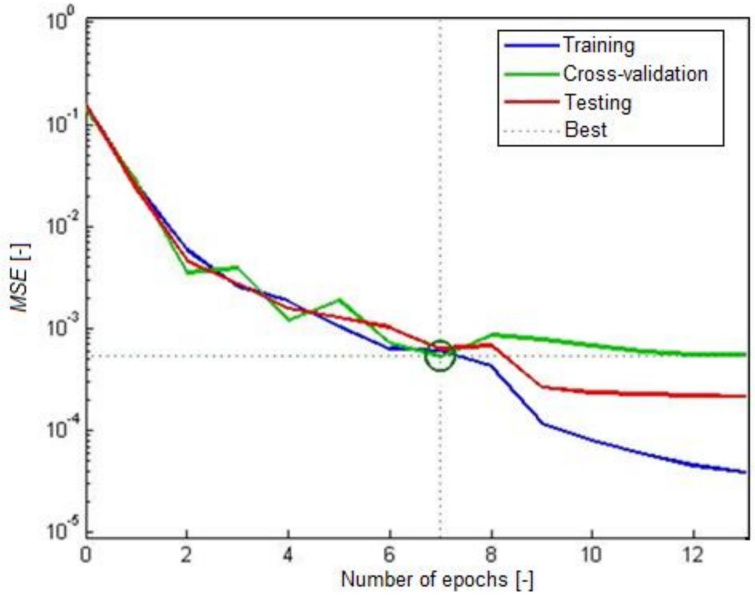

Figure 7. Performance in the FA-ANN with the optimum 8-8-4-1 structure.

3.2. Results of Learning, Testing and Cross-Validation of the FA-ANN

Figure 8 illustrates the training state of the FA-ANN. According to this figure, the errors were repeated 6 times after epoch number 7, and the acting was stopped at epoch 13. In other words, the last epoch before the error repetitions, namely epoch 7, was considered as the best performance and its

related weights were assumed as the final model weights. Furthermore, the cross-validation check was equal to 6 since it was based on the number of repetitions.

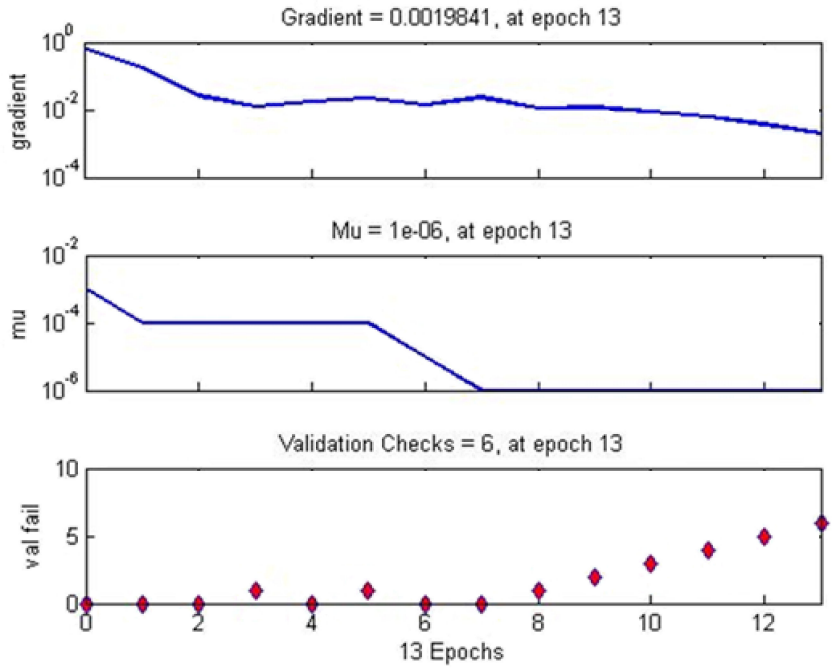

Figure 8. State in the FA-ANN with optimum 8-8-4-1 structure.

Figure 9 shows the relative error (RE) distribution histogram of the FA-ANN for the training, cross-validation and testing steps. This figure shows that the data fitting errors were distributed within a reasonably satisfactory range around zero.

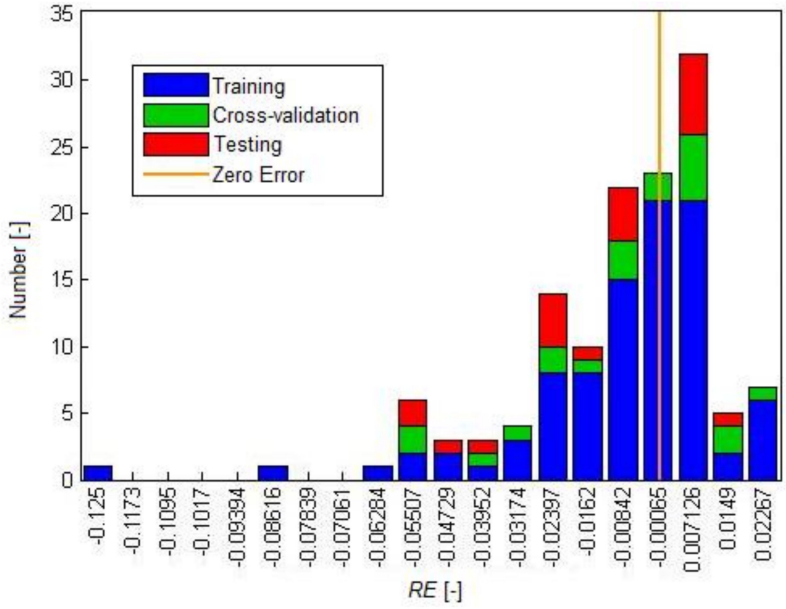

Figure 9. Error (*RE*) distribution at different stages of the FA-ANN with optimum 8-8-4-1 structure.

3.3. Validation of the FA-ANN Model

In order to evaluate the accuracy of the FA-ANN model, it was compared with the other commonly used algorithms, such as the genetic algorithm (GA), imperialist competitive algorithm (ICA) and

particle swarm optimization (PSO). The characteristics of these algorithms, used for validation of the FA-ANN model, are given in Table 7.

Table 7. The characteristics of the Firefly Algorithm (FA), Genetic Algorithm (GA), imperialist competitive algorithm (ICA) and particle swarm optimization (PSO) algorithms used for validation.

FA		*GA*		*ICA*		*PSO*	
Attraction coefficient	0.5	Population	150	Number of initial countries	500	Swarm size	100
Mutation coefficient	0.9	Mutation rate	15	Number of initial imperialists	50		
Number of fireflies	10	Crossover rate	50	Assimilation angle coefficient(β)	2	Cognition coefficient	2
Radius reduction factor	0.95			Angle coefficient (γ)	0.5	Social coefficient	2
Generation	50	Generation	50	Generation	50	Generation	50

Figure 10 indicates the comparison of experimental and computational values for the creep strain parameter using the ANN model modified by the FA, ICA, GA and PSO. The results presented indicated that the ANN model optimized by the FA determined the creep strain values more accurately than other algorithms. This has been stated on the basis of the comparison of the values of linear correlation coefficient *R*, mean absolute error *MAE*, mean squared error *MSE* and root mean square error *RMSE*.

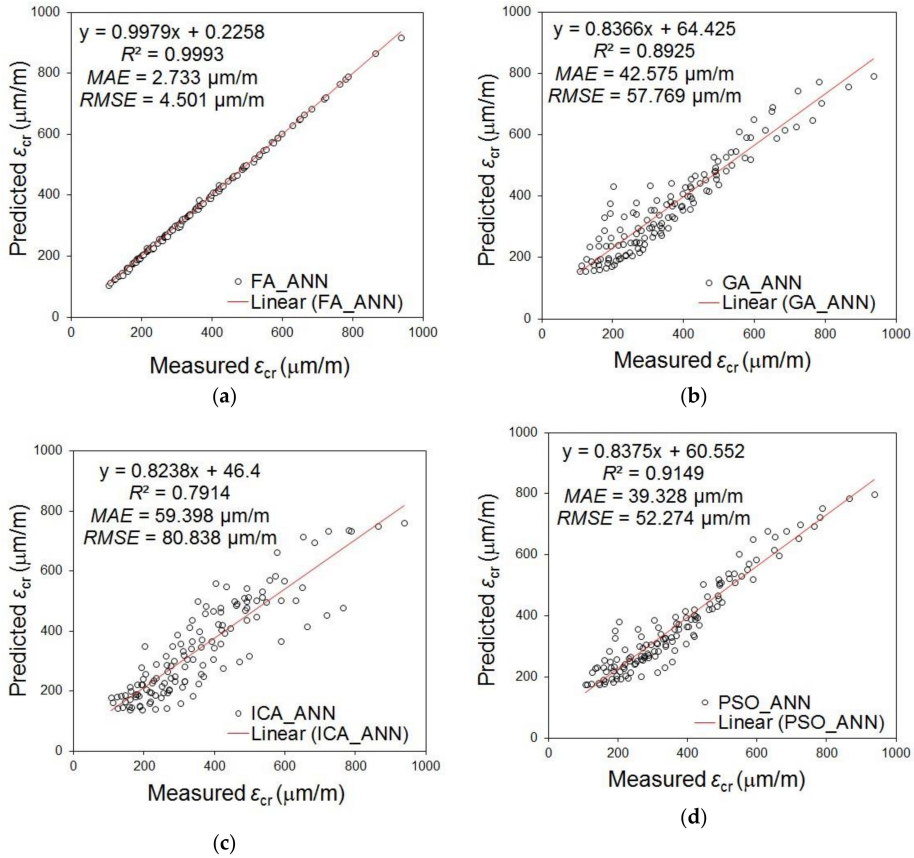

Figure 10. Results of experimental and computational values for the creep strain parameter using the ANN model modified by: (**a**) FA; (**b**) GA; (**c**) ICA; (**d**) PSO.

4. Conclusions

The conclusions drawn from the above analysis for the prediction of the creep strain of GGBFS concrete are as follows:

- It is possible to predict the creep strain of green concrete with GGBFS using artificial neural networks (ANN) and the nature-inspired metaheuristic firefly algorithm (FA).

- A reliable prediction can be conducted based on the parameters of GGBFS concrete, which characterize the composition of the concrete mixture and selected rheological properties. For this purpose, the cement content, GGBFS content, water-to-binder ratio, fine aggregate content, coarse aggregate content, slump, the compaction factor of concrete and the age after loading were used as the input parameters, and in turn the creep strain (ε_{cr}) of GGBFS concrete was considered as the output parameter.
- The ANN model optimized by the FA was able to predict the value of ε_{cr} with a very high level of accuracy. The obtained values of determination coefficient (R^2) were equal to 0.99 in training, cross-validation and testing.
- The performance of the FA-ANN was compared with other commonly used algorithms such as the imperialist competitive algorithm (ICA), genetic algorithm (GA) and particle swarm optimization (PSO). The obtained results indicated that the ANN model optimized by the FA was more accurate and provided more precision than other models.

Author Contributions: Methodology, M.N.,M.S. and E.J.; numerical analysis, M.N. and E.J.; experimental tests M.S.; writing—original draft preparation, L.S., M.S. and S.C.; writing—review and editing, S.C. and L.S.; supervision, L.S.

Funding: This research received funding from project no. 0402/0091/18 entitled "Application of artificial intelligence to assess physical properties of selected building materials [Zastosowanie sztucznej inteligencji do oceny cech fizycznych wybranych materiałów budowlanych]" funded by the Ministry of Science and Higher Education in Poland (decision no. 8763/E-366/M/2018).

Conflicts of Interest: The authors declare no conflicts of interest.

References

1. El-Shafie, A.; Aminah, S. Dynamic versus static artificial neural network model for masonry creep deformation. *Proc. Inst. Civ. Eng.-Struct. Build.* **2013**, *166*, 355–366. [CrossRef]
2. Hołowaty, J. Creep and Shrinkage of Concrete in Eurocode 2 and Polish Bridge Standards—Necessity for Implementation. *J. Civ. Eng. Arch.* **2015**, *9*, 460–466. [CrossRef]
3. Özbay, E.; Erdemir, M.; Durmuş, H.İ. Utilization and efficiency of ground granulated blast furnace slag on concrete properties—A review. *Constr. Build. Mater.* **2016**, *105*, 423–434. [CrossRef]
4. Barnett, S.J.; Soutsos, M.N.; Millard, S.G.; Bungey, J.H. Strength development of mortars containing ground granulated blast-furnace slag: Effect of curing temperature and determination of apparent activation energies. *Cem. Concr. Res.* **2006**, *36*, 434–440. [CrossRef]
5. Young, C.H.; Chern, J.C. Practical prediction model for shrinkage of steel fibre reinforced concrete. *Mater. Struct.* **1991**, *24*, 191–201. [CrossRef]
6. Han, M.Y.; Lytton, R.L. Theoretical prediction of drying shrinkage of concrete. *ASCEJ. Mater. Civ. Eng.* **1995**, *7*, 204–207. [CrossRef]
7. Kim, J.K.; Lee, C.S. Prediction of differential drying shrinkage in concrete. *Cem. Concr. Res.* **1998**, *28*, 985–998. [CrossRef]
8. Bazant, Z.P. Prediction of concrete creep and shrinkage: Past, present and future. *Nucl. Eng. Des.* **2001**, *203*, 27–38. [CrossRef]
9. Eguchi, K.; Teranishi, K. Prediction equation of drying shrinkage of concrete based on composite model. *Cem. Concr. Res.* **2005**, *35*, 483–493. [CrossRef]
10. Gardner, N.J. Design provisions for drying shrinkage and creep of normal strength concrete. *ACI Mater. J.* **2001**, *98*, 159–167.
11. Shariq, M.; Prasad, J.; Abbas, H. Creep and drying shrinkage of concrete containing GGBFS. *Cem. Concr. Compos.* **2016**, *68*, 35–45. [CrossRef]
12. Karthikeyan, J.; Upadhyay, A.; Bhandari, N.M. Artificial neural networks for predict creep and shrinkage of high performance concrete. *J. Adv. Concr. Technol.* **2008**, *6*, 135–142. [CrossRef]
13. Gedam, B.A.; Bhandari, N.M.; Upadhyay, A. An apt material model for drying shrinkage and specific creep of HPC using artificial neural network. *Struct. Eng. Mech.* **2014**, *52*, 97–113. [CrossRef]

14. Bal, L.; Bodin, F.B. Artificial neural network for predicting creep of concrete. *Neural Comput. Appl.* **2014**, *25*, 1359–1367. [CrossRef]
15. Freidriks, A. Prediction models of shrinkage and creep in industrial floors and overlays, Degree Project. In *Division of Concrete Structures*; Second Level; KTH Royal Institute of Technology: Stockholm, Sweden, 2015.
16. Asteris, P.G.; Roussis, P.C.; Douvika, M.G. Feed-Forward Neural Network Prediction of the Mechanical Properties of Sandcrete Materials. *Sensors* **2017**, *17*, 1344. [CrossRef] [PubMed]
17. Cheng, M.Y.; Hoang, N.D. A self-adaptive fuzzy inference model based on least squares SVM for estimating compressive strength of rubberized concrete. *Int. J. Inf. Technol. Decis. Mak.* **2016**, *15*, 603–619. [CrossRef]
18. Khademi, F.; Akbari, M.; Jamal, S.M.; Nikoo, M. Multiple linear regression, artificial neural network, and fuzzy logic prediction of 28 days compressive strength of concrete. *Front. Struct. Civ. Eng.* **2017**, *11*, 90–99. [CrossRef]
19. Khademi, F.; Akbari, M.; Nikoo, M. Displacement Determination of Concrete Reinforcement Building using Data-Driven models. *Int. J. Sustain. Built Environ.* **2017**, *6*, 400–411. [CrossRef]
20. Golafshani, E.M.; Behnood, A. Application of soft computing methods for predicting the elastic modulus of recycled aggregate concrete. *J. Clean. Prod.* **2018**, *176*, 1163–1176. [CrossRef]
21. Golafshani, E.M.; Behnood, A. Automatic regression methods for formulation of elastic modulus of recycled aggregate concrete. *Appl. Soft Comput.* **2018**, *64*, 377–400. [CrossRef]
22. Erzin, Y.; Nikoo, M.; Nikoo, M.; Cetin, T. The use of self-organizing feature map networks for the prediction of the critical factor of safety of an artificial slope. *Neural Netw. World* **2016**, *26*, 461–476. [CrossRef]
23. Gandomi, A.H.; Sajedi, S.; Kiani, B.; Huang, Q. Genetic programming for experimental big data mining: A case study on concrete creep formulation. *Autom. Construct.* **2016**, *70*, 89–97. [CrossRef]
24. IztokFister, I.F., Jr.; Yang, X.-S.; Brest, J. A comprehensive review of firefly algorithms. *Swarm Evolut. Comput.* **2013**, *13*, 34–46. [CrossRef]
25. Yang, X.-S. Firefly Algorithm. In *Engineering Optimization*; John Wiley: Hoboken, NJ, USA, 2010; Volume 17.
26. Bui, D.K.; Nguyen, T.; Chou, J.S.; Nguyen-Xuan, H.; Ngo, T.D. A modified firefly algorithm-artificial neural network expert system for predicting compressive and tensile strength of high-performance concrete. *Construct. Build. Mater.* **2018**, *180*, 320–333. [CrossRef]
27. Sheikholeslami, R.; Khalili, B.G.; Sadollah, A.; Kim, J. Optimization of reinforced concrete retaining walls via hybrid firefly algorithm with upper bound strategy. *KSCE J. Civ. Eng.* **2016**, *20*, 2428–2438. [CrossRef]
28. Nigdeli, S.M.; Bekdaş, G.; Yang, X.S. Metaheuristic optimization of reinforced concrete footings. *KSCE J. Civ. Eng.* **2018**, *22*, 1–9. [CrossRef]
29. IS 8112. *43 Grade Ordinary Portland Cement—Specification*; Bureau of Indian Standards: New Delhi, India, 1989.
30. IS 12089. *Indian Standard Specification for Granulated Slag for Manufacture of Portland Slag Cement*; Bureau of Indian Standards: New Delhi, India, 1999.
31. Shariq, M. Studies in Creep Characteristics of Concrete and Reinforced Concrete. Ph.D. Thesis, IIT Roorkee, Roorkee, India, 2008.
32. IS 516. *Indian standard: Methods of Tests for Strength of Concrete*; Bureau of Indian Standards: New Delhi, India, 1999.
33. Shariq, M.; Prasad, J.; Masood, A. Effect of GGBFS on time dependent compressive strength of concrete. *Construct. Build. Mater.* **2010**, *24*, 1469–1478. [CrossRef]
34. Shapiro, S.; Wilk, M. An analysis of variance test for normality. *Biometrika* **1965**, *52*, 591–611. [CrossRef]
35. Snedecor, G.W. *Calculation and Interpretation of Analysis of Variance and Covariance*; Collegiate Press, Inc.: Ames, Iowa, 1934.
36. Bažant, Z.P.; Jirásek, M. *Creep and Hygrothermal Effects in Concrete Structures*; Springer: Berlin, Germany, 2018; Volume 225.
37. Hecht-Nielson, R. Kolmogorov's mapping neural network existence theorem. In Proceedings of the First IEEE International Joing Conference on Neural Networks, San Diego, CA, USA, 13–17 July 1987.
38. Rogers, L.L.; Dowla, F.U. Optimization of groundwater remediation using artificial neural networks with parallel solute transport modeling. *Water Resour. Res.* **1994**, *30*, 457–481.